# Structure and Dynamics of Structure Formation in Model Triarm Star Block Copolymers of Polystyrene, Poly(ethylene oxide), and Poly($\epsilon$-caprolactone)

**G. Floudas***

*Foundation for Research and Technology−Hellas (FORTH), Institute of Electronic Structure and Laser, P.O. Box 1527, 711 10 Heraklion Crete, Greece*

**G. Reiter, O. Lambert, and P. Dumas**

*Institut de Chimie des Surfaces et Interfaces, 15 rue Jean Starcky, B.P. 2488, 68057 Mulhouse Cedex, France*

*Received April 27, 1998; Revised Manuscript Received August 19, 1998*

ABSTRACT: The structure and dynamics of structure formation have been studied in model triarm star block copolymers composed of two crystallizable blocks (poly(ethylene oxide) (PEO) and poly($\epsilon$-caprolactone) (PCL)) and one amorphous block (polystyrene (PS)). Crystallization starts from the homogeneous phase. For the structure investigation, X-ray scattering, optical microscopy, and atomic force microscopy have been employed, whereas for the kinetics, we have used differential scanning calorimetry, optical microscopy, and rheology. In the stars, there is a competition for crystallization between the two crystallizable blocks which have similar mobilities and melting temperatures but crystallize in different unit cells (monoclinic vs orthorhombic). When the crystallizable block length ratio is 3 or higher, only the longer block will crystallize. For comparable lengths both blocks can crystallize—however, not within the same molecule—but the crystallinity, long period, and crystalline lamellar thickness are reduced with respect to the pure PEO and PCL. The latent heats, obtained in the isothermal crystallization calorimetric experiments, are analyzed in terms of the Avrami theory. Although similar Avrami exponents were found for all stars ($n = 2$, reflecting a disklike growth from heterogeneous nuclei), the crystallization times were different depending on the nature of the crystallizable blocks. Optical microscopy revealed the formation of different superstructures (spherulites/axialites) depending on the type of crystallizable block (PEO/PCL). The growth rates of these superstructures were obtained and analyzed in terms of a kinetic nucleation theory, and the fold surface free energies were extracted. Notwithstanding the larger specific surface of bulk PCL as compared to that of PEO, the fold surface free energies in the stars were similar to that in PEO, indicating a pure PEO crystal and mixing of the amorphous blocks with the PCL crystal. This is supported from the results of the atomic force microscopy measurements on thin films, which have indicated the formation of perforated PCL crystals.

## Introduction

The process of crystallization is of fundamental importance to the applications of semicrystalline homopolymers. For example, the final optical and mechanical properties of polymers are controlled by the size of spherulites and overall crystallinity, which are again controlled by the type of nucleation, the growth rate, and the characteristics of the individual folded chains (i.e., fold surface free energies). The structure and dynamics of structure formation (crystallization) in semicrystalline polymers have been studied extensively.[1,2] Recently, such polymers have been combined with amorphous polymers to form crystalline/amorphous diblock copolymers. Block copolymers composed of two amorphous blocks exhibit a rich phase behavior which is controlled by the volume fraction ($f$), the product of the interaction parameter ($\chi$) with the total degree of polymerization ($N$), and the architecture.[3,4] The thermodynamic interaction parameter can be effectively triggered by a suitable combination of amorphous and semicrystalline polymers. Block copolymers composed of amorphous and crystallizable blocks enable the preparation of nanoscale semicrystalline materials, i.e., materials with enhanced mechanical properties. Furthermore, such materials can develop structure over a range of length scales, from the unit cell structure of the crystalline block to the microdomain length scale to the spherulitic scale.

Although such block copolymers have been synthesized and investigated mainly by scattering techniques,[5−11] the effect of chain topology and architecture on block copolymer crystallization is totally unexplored. Furthermore, there are only a very few studies on block copolymers composed of two crystallizable blocks. In the first such study by Skoulios et al.,[12] the structure of triblock copolymers of poly($\epsilon$-caprolactone)−poly(ethylene oxide)−poly($\epsilon$-caprolactone) (PCL−PEO−PCL) was investigated. In these linear block copolymers, both blocks were able to crystallize. In a more recent study,[13] diblocks of PEO and PCL rich in PCL were investigated. In the latter system only the PCL block could crystallize.

Recently, the synthesis of model triarm star block copolymers (known also as heteroarm or miktoarm stars) composed of two crystallizable blocks and one amorphous block has been reported.[14] Such materials provide the possibility of triggering the thermodynamic parameters and altering the phase state using known blocks but combined to form a new architecture. An obvious application of these new materials would be as combatibilizers of amorphous and semicrystalline blocks. In fact, they can combatibilize two semicrystalline blocks with an amorphous one. Such a system, how-

10.1021/ma9806716 CCC: $15.00 
Published on Web 10/02/1998

**Table 1. Molecular Characteristics of the Homopolymers, Diblocks, and Triarm Star Block Copolymers**

| sample | $M_n$(PS) $\times 10^3$ | $M_n$(PEO) $\times 10^3$ | $M_n$(PCL) $\times 10^3$ | $M_n$(total) $\times 10^3$ | $M_w/M_n$ |
|---|---|---|---|---|---|
| PEO | | 15 | | 15 | 1.3 |
| PCL10 | | | 10 | | |
| PCL42 | | | 42.5 | | 1.45 |
| PEO−PCL | | 15 | 5 | 20 | 1.5 |
| PS−PEO | 4.7 | 20 | | 24.7 | 1.16 |
| SEL-4.7/20/1.8 | 4.7 | 20 | 1.8 | 27 | 1.15 |
| SEL-4.7/20/10 | 4.7 | 20 | 10 | 35 | 1.27 |
| SEL-4.7/20/45 | 4.7 | 20 | 45 | 70 | 1.19 |
| SEL-4.7/20/87 | 4.7 | 20 | 87 | 112 | 1.29 |

ever, is very complex by construction. An ABC star block copolymer comprised of two semicrystalline blocks (A and B) and an amorphous block (C) contains three amorphous phases (with the corresponding glass transition temperatures $T_g^A$, $T_g^B$, and $T_g^C$) and two crystalline phases (with the corresponding equilibrium melting temperatures $T^\circ_{m,A}$ and $T^\circ_{m,B}$). In addition, there will be another temperature of interest, namely, the order-to-disorder transition temperature for the block copolymer. Moreover, in the most general case, three interaction parameters are needed to predict the phase behavior: $\chi_{AB}$, $\chi_{BC}$, and $\chi_{AC}$. Clearly, such a system, despite being attractive, is not the best to start such an investigation.

For the present investigation we are employing one of the simplest possible star block copolymers composed of two crystallizable blocks. The crystallizable blocks are PEO and PCL, which are sensitive probes of crystallization, and the amorphous block is polystyrene (PS). This system is much simpler; the glass transition and equilibrium melting temperatures of PEO and PCL are similar. Moreover, PS and PCL are compatible in the melt state,[15,16] and the star structure with PEO is likely to increase the intrinsic compatibility of the system.[4,17,18] However, despite these similarities, PEO and PCL have some differences, which make the choice of the system a unique one: they crystallize in different unit cells[19,20] (monoclinic vs orthorhombic), have distinctly different specific area requirements for their folded chains ($\sigma_e^{PCL} \gg \sigma_e^{PEO}$, where $\sigma_e$ is the fold surface free energy), and form different superstructures (spherulites vs axialites). This richness in the crystal structures of PEO and PCL, ranging from the unit cell to the crystal superstructure, is of primary importance for the present investigation and is used as a fingerprint for the crystallizable block. Herein, we investigate the structure and dynamics of structure formation in a series of model star block copolymers based on PS, PEO, and PCL using X-rays, calorimetry, rheology, optical microscopy, and atomic force microscopy.

## Experimental Section

**Materials.** The homopolymers (PEO and PCL) and diblock copolymers (PEO−PCL and PS−PEO) were synthesized by anionic polymerization following standard procedures. Triarm star block copolymers were obtained by two successive initiation steps on a bifunctional macroinitiator.[14] This route of synthesis avoided reaction between polymeric species and thus led to well-defined triarm star block copolymers of high molecular weight (up to 260 000) without containing any measurable amounts of homopolymers or diblock copolymers. The molecular characteristics of the block copolymer stars are given in Table 1. Details on the synthesis and characterization can be found elsewhere.[14]

**Optical Microscopy.** Thin films (30−200 nm) of the samples were prepared by spin-coating from dried toluene solutions. Solutions were spread out by centrifugal force, resulting in a micrometer thick film of solution. A smooth solid polymer film was formed by evaporating the solvent. These samples were then introduced into a hotplate, purged with nitrogen, under a Leitz-Metallux 3 optical microscope. No polarization or phase contrast was used. Contrast is due to the interference of the reflected light at the substrate/film and film/air interface. We have followed the growth of spherulites in real time by capturing the images by a CCD camera. The kinetic experiments were made by making *T*-jumps from a temperature in the range 343−353 K (i.e., only a few degrees above the melting point). This was necessary in order to reduce the cooling period and to use self-seeding for the nucleation process. At the final crystallization temperatures, we have followed the diameter of the spherulites and the long and short axes of axialites (see below) as a function of time to obtain the growth rates.

**X-ray Scattering.** Both WAXS and SAXS measurements have been performed. The WAXS measurements were carried out with a Siemens $\theta-\theta$ diffractometer (Model D500T) in the reflection geometry. The Cu K$\alpha$ radiation was used from a Siemens generator (Kristalloflex 710 H) operating at 35 kV and 30 mA, and a graphite monochromator was utilized in front of the detector ($\lambda = 0.154$ nm). Measurements were made in the $2\theta$ range from 4 to 60° in steps of 0.01°. We have used the following thermal history: samples were first heated above the melting temperature (to erase any history) and slowly cooled to room temperature, where they were given sufficient time to crystallize. All measurements were made by heating from ambient temperature to the melting temperature. The scattering profiles at the two highest temperatures are shown in Figure 1.

**Differential Scanning Calorimetry (DSC).** A Polymer Laboratories DSC capable of programmed cyclic temperature runs over the range 113−673 K was used. Isothermal kinetic experiments have been performed to follow the crystallization of the crystallizable components in the stars. First the samples were heated to a temperature ($T_i = 348$ K) located well above the equilibrium melting points of all samples. Then we performed *T*-jumps to different final temperatures with a cooling rate of 10 K/min. The final temperatures were in the range 314−319 K for the samples PS−PEO, SEL-4.7/20/1.8, and SEL-4.7/20/87 and in the range 309−314 K for SEL-4.7/20/45. During the crystallization process, we monitored the time dependence of the (single) exothermal peak. After the completion of the crystallization process, the samples were heated to the initial temperature (348 K) at 10 K/min. During heating we obtained the apparent melting temperatures from the peak of the endothermal processes. These apparent melting temperatures were subsequently corrected for the heating rate. For this purpose all samples were crystallized at 303 K from the initial temperature, and the apparent melting temperatures were obtained by using different heating rates: 0.2, 0.5, 1, 2, 5, and 10 K/min. The apparent melting temperature at this crystallization temperature was obtained by linear extrapolation. Typically, a heating rate of 10 K/min results in a higher apparent melting temperature as

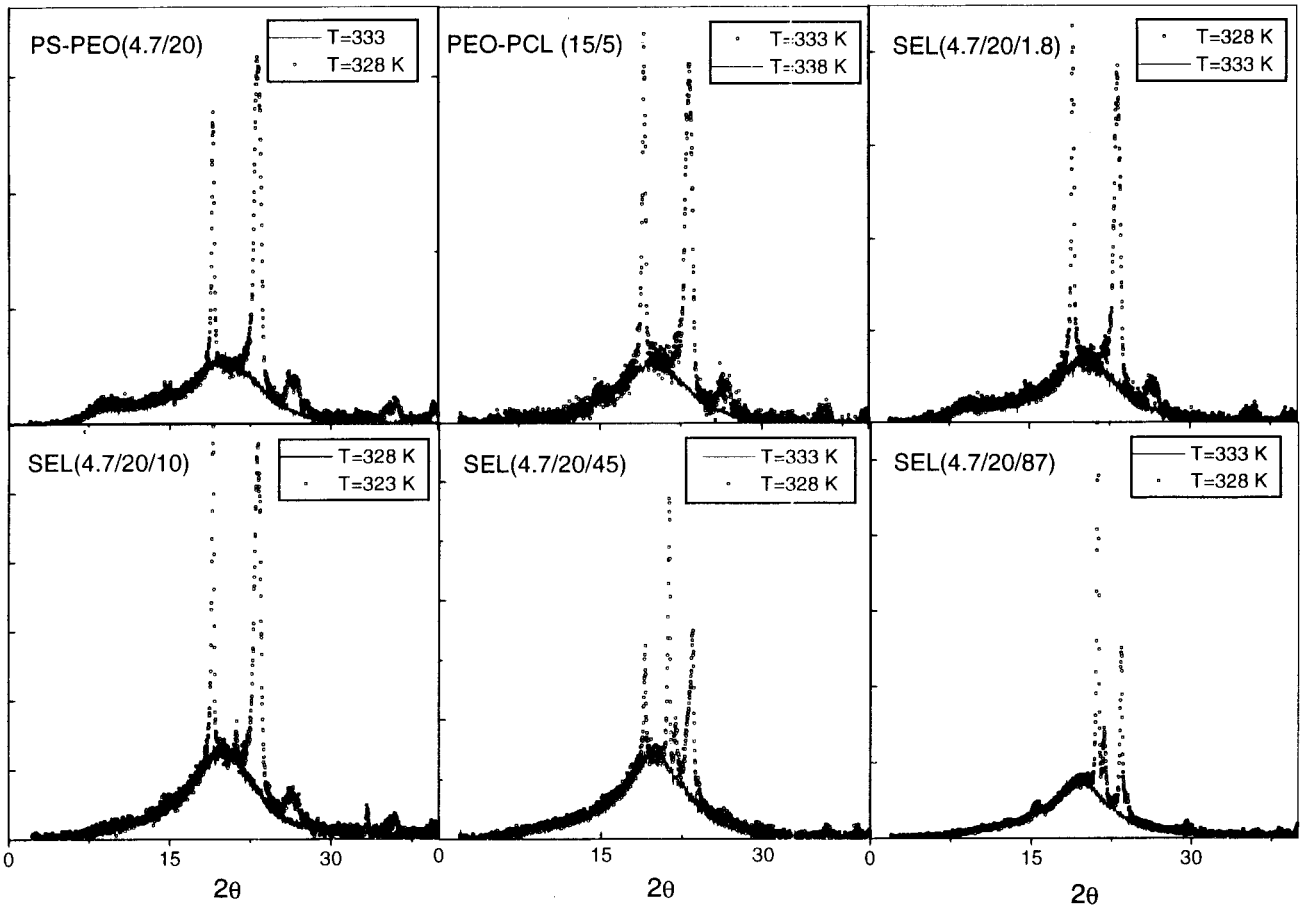


**Figure 1.** Wide-angle X-ray scattering intensity profiles for the two diblocks PS−PEO and PEO−PCL and four of the star block copolymers at two temperatures as indicated: (○) below the equilibrium melting point; (solid line) $T$ above the melting point. Notice that the Bragg reflections for the SEL-4.7/20/87 sample correspond to the PCL lattice of the crystal structure (orthorhombic) and those for PS−PEO, PEO−PCL, and SEL-4.7/20/1.8 to the PEO lattice (monoclinic). For SEL-4.7/20/10 and SEL-4.7/20/45, there are two sets of Bragg reflections corresponding to the lattices of both PEO and PCL.

compared to the slowest heating rate of 0.2 K/min of about 3 K. Subsequently, all apparent melting points were corrected for the effect of heating rate.

**Rheology.** An advanced rheometric expansion system (ARES) equipped with a force-rebalanced transducer was used in the oscillatory mode to measure the storage ($G'$) and loss ($G''$) moduli. A parallel-plate sample geometry was used with a diameter of 8 mm and a sample thickness of about 1 mm. Two types of experiments have been performed: (i) isochronal temperature heating and cooling scans at $\omega = 1$ rad/s with a heating rate of 0.3 K/min and (ii) isochronal/isothermal time scans at $\omega = 1$ rad/s and different final temperatures as in the DSC experiments. In particular, the slow heating rate in the former experiment was chosen to be comparable with the heating rate used in the DSC experiments for the determination of the apparent and equilibrium melting temperatures.

**Atomic Force Microscopy (AFM).** Measurements were performed with a Nanoscope IIIa (Digital Instruments) in the tapping mode at ambient conditions. We used Si tips on cantilevers with a resonant frequency of about 300 kHz. Scan rates were between 0.2 and 1 Hz. Topographic (height mode) and viscoelastic (phase mode) measurements were simultaneously recorded. It should be noted that semicrystalline polymers are well suited for the use of the "phase mode" since the differences in viscoelastic properties between crystalline and amorphous regions are large. All samples were first crystallized under an optical microscope at a constant temperature.

## Results and Discussion

**Structure.** The structure and phase state of the stars have been investigated by SAXS, WAXS, and synchrotron simultaneous SAXS/WAXS measurements. The absence of higher order reflections in the SAXS data revealed that the stars form a homogeneous phase in the melt.[21] Hence, crystallization in these systems starts from the homogeneous melt. This finding is not surprising given the compatibility of PS with PCL[15,16] and the star architecture which enhances the compatibility of the blocks;[4,17,18] i.e., $(\chi N)_{star} > (\chi N)_{diblock}$, which implies that the $T_{ODT}$ of a star is lower than that for a diblock made of the same blocks. Some representative WAXS spectra for the different samples are shown in Figure 1. It is evident that, depending on the block length ratio, different Bragg reflections are present in the spectra. The crystal structure of PEO is monoclinic[19] with a unit cell parameter of 1.93 nm along the helix axis, whereas PCL is orthorhombic[20] and the chains assume a planar all-trans conformation. Therefore, the Bragg reflections of the two polymer crystals are distinctly different, and this structural property will be used as a fingerprint of the crystallizable block and its crystallinity. In the PS−PEO and PEO−PCL diblocks as well as in the star SEL-4.7/20/1.8, the Bragg reflections correspond solely to the PEO crystals. Alterna-

tively, in SEL-4.7/20/87 the Bragg reflections are characteristic of PCL crystals. For the stars with comparable block lengths for the two crystallizable components, the WAXS spectra show mixed reflections, indicating the existence of both PEO *and* PCL crystals. On the basis of the WAXS patterns, we conclude that in the stars with a crystallizable block length ratio of 3 or higher the longer block completely suppresses the crystallization of the shorter one. However, when the block length ratio is less than 3, then both blocks can undergo crystallization.

This suppression of crystallization in the stars, where only the longer block can crystallize, is at first glance surprising. Based on thermodynamics, at a given (low) crystallization temperature the thermodynamic driving forces for crystallization of PEO and PCL are not very different given the similarity in the equilibrium melting points (see below). Furthermore, the growth rate of the PEO crystals is higher than that of the PCL crystals (see below), so on the basis of the equilibrium melting temperatures and the growth rates alone, one would expect that the PEO blocks always crystallize. However, this is not the case in SEL-4.7/20/87, where the longer (PCL) block suppresses completely the PEO crystallization. It is plausible that the longer block offers more nucleation sites for the heterogeneous nucleation process (see below with respect to the kinetics), which upon crystallization restricts the available space for the crystallization of the second block. In this picture, spatial restrictions suppress the crystallization of the shorter block.

On the basis of the WAXS data, we can obtain the weight fraction of crystallinity $X_c$ of PEO and/or PCL from the area under the corresponding crystalline reflections ($I_c$) and the amorphous halo ($I_a$) from

$$X_c = \frac{I_{c,i}}{I_{c,i} + wI_a} \quad (1)$$

where $I_{c,i}$ represents the crystalline intensity from one of the components and $w$ is the weight fraction of PEO or PCL. Equation 1 is approximate; it assumes the same scattering efficiency for the amorphous and crystalline material and ignores the diffuse scattering due to crystal lattice imperfections and vibrations. The crystallinities obtained in this way are plotted in Figure 2 as a function of the block ratio of the crystallizable blocks $N^{PCL}/N^{PEO}$. The crystallinities in the PS−PEO and PEO−PCL diblocks (which are not shown in Figure 2) are 51 and 46%, respectively. In the stars, the crystallinity is reduced considerably; the most dramatic reduction occurs for PCL under conditions where both blocks crystallize. In these cases (samples SEL-4.7/20/10 and SEL-4.7/20/45) the crystallinity of the PCL phase is below 20%. As we will discuss later with respect to the kinetic studies, the reduction is associated with mixing within the PCL phase.

The long period (i.e., the average distance of lamellar crystals separated by amorphous regions) and crystal thickness were also found to be affected in the stars relative to the pure components. The results shown in Figure 3 give the long period $D$ ($=2\pi/Q^*$) for the diblocks and the star block copolymers as a function of the ratio of the degrees of polymerization of the amorphous and crystalline parts. The main peak at $Q^*$ was extracted from the Lorentz-corrected SAXS data which are shown in the inset. The number of chain folds can be obtained

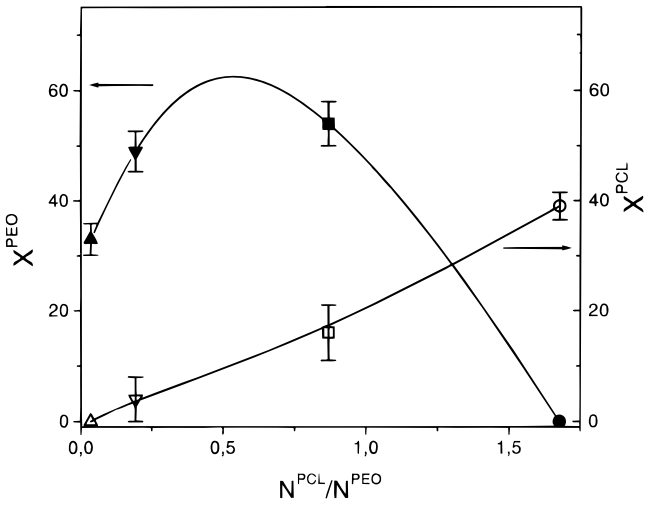


**Figure 2.** Weight fraction of PEO (filled symbols) and PCL (open symbols) crystallinity plotted as a function of the ratio of the degrees of polymerization $N^{PCL}/N^{PEO}$: (△) SEL-4.7/20/1.8, (▽) SEL-4.7/20/10, (□) SEL-4.7/20/45, (○) SEL-4.7/20/87.

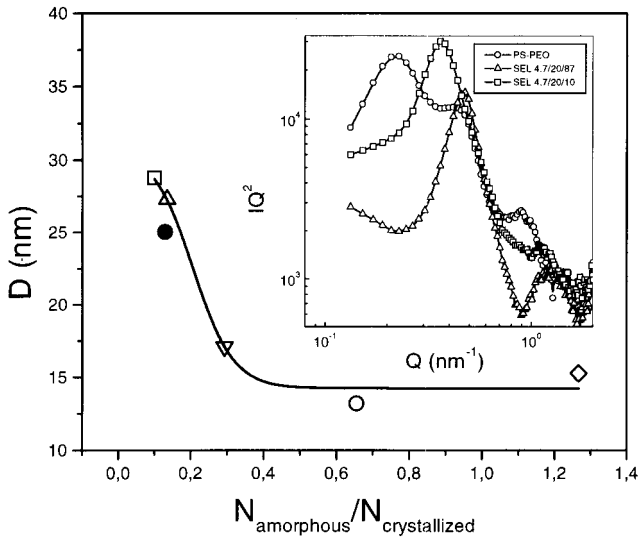


**Figure 3.** Long period obtained from the SAXS peak of the Lorentz-corrected data (shown in the inset for three samples), as a function of the ratio of the degrees of polymerization of the amorphous and crystallized blocks: (●) PEO−PCL (15/5), (□) PS−PEO (4.7/20), (△) SEL-4.7/20/1.8, (▽) SEL-4.7/20/10, (○) SEL-4.7/20/87, (◇) SEL-4.7/20/45.

from the thickness of a fully extended (integral folding (IF) = 0) PEO chain ($\lambda_{max} = (M_n^{PEO}/M_n^{EO}) \times 0.278$ nm). The values for the total thickness of the crystalline domains and the crystalline lamellar thickness of PEO, $\lambda$, are given in Table 2. For the calculation of the PEO crystalline lamellar thickness, we have used the Gibbs−Thomson equation,[1,2,22] which relates the melting point depression to $\lambda$:

$$T_m^{0\prime} = T_m^0\left(1 - \frac{2\sigma_e}{\Delta H_f}\frac{1}{\lambda}\right) \quad (2)$$

where $T_m^{0\prime}$ and $T_m^0$ are the equilibrium melting points in the stars (see below) and in the bulk PEO ($T_m^0$ = 343 K), respectively, $\sigma_e$ is the fold surface free energy, and $\Delta H_f$ is the heat of fusion (230 J/cm$^3$).[22] The results for the long period (Figure 3) and the crystalline lamellar thickness (Table 2) reveal that in the stars the long period and crystal thickness are substantially

**Table 2. Structural Parameters of the Diblocks and Triarm Star Block Copolymers**

| sample | long period (nm)[a] | PEO domain thickness $d_{PEO}$ (nm)[b] | PCL domain thickness $d_{PCL}$ (nm)[b] | total thickness of crystalline PEO phase $d_c$ (nm)[c] | crystalline lamellar thickness $\lambda_{PEO}$ (nm)[d] |
|---|---|---|---|---|---|
| PEO−PCL-15/5 | 24.4 | 21.7 | | 11.1 | |
| PS−PEO-4.7/20 | 28.8 | 25.9 | | 14.7 | 7.2 |
| SEL-4.7/20/1.8 | 27.3 | 24 | | 8.7 | 6.3 |
| SEL-4.7/20/10 | 17.1 | 13.1 | 2.6 | 6.1 | 6.4 |
| SEL-4.7/20/45 | 15.3 | 7.8 | 6.7 | 2.9 | |
| SEL-4.7/20/87 | 13.2 | | 7.9 | | |

[a] From the SAXS peak as $D = 2\pi/Q^*$. [b] Calculated from $d_{PEO} = \varphi_{PEO}D$ ($\varphi_{PEO}$ defined as $N_{PEO}/(N_{PEO} + N_{PCL})$). [c] Caclulated from $d_c = X_c^{DSC}d_{PEO}$. [d] From the Gibbs−Thomson equation.

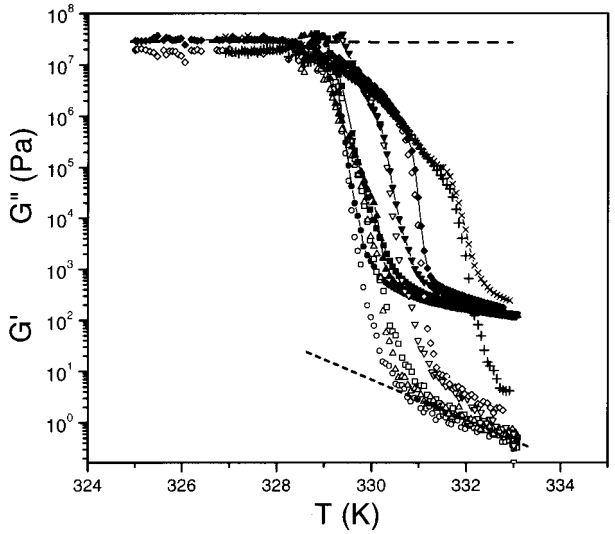


**Figure 4.** Isochronal measurements ($\omega$ = 1 rad/s) of the storage modulus $G'$ (open symbols) and loss modulus $G''$ (filled symbols) of SEL-4.7/20/1.8 obtained during heating (heating rate: 0.3 K/min) following the crystallization at different temperatures $T$ (K): (○) 321, (□) 322, (△) 323, (▽) 324, (◇) 325, (+) 326. The lines give the $T$ dependence of $G'$ of the spherulitic and melt phases, at some crystallization temperatures.

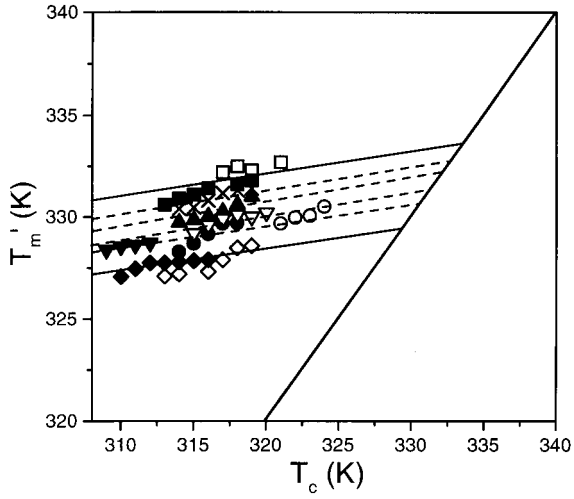


**Figure 5.** Hoffman−Weeks plot used in the determination of the equilibrium melting point. The apparent melting points are determined from DSC (filled symbols) and rheology (open symbols): (squares) PCL, (triangles) PS−PEO, (circles) SEL-4.7/20/1.8, (×) SEL-4.7/20/87, (down triangles) SEL-4.7/20/45, (rhombuses) SEL-4.7/20/10. The solid line is the line $T_m' = T_c$.

reduced and the magnitude of the reduction depends on the ratio $N_{amorphous}/N_{crystallized}$.

Use of eq 2 to obtain the crystalline lamellar thickness requires knowledge of the fold surface free energies and the equilibrium melting temperatures. To obtain the surface free energies, we have employed optical microscopy, whereas for the equilibrium melting temperatures, calorimetry and rheology have been used. DSC is a commonly used method to determine equilibrium melting temperatures; recently it has been shown that rheology can also be used for the same purpose.[11] In DSC, we have monitored the time dependence of crystallization at different temperatures and then performed heating runs with different heating rates in order to extract the apparent melting temperatures from the position of the (single) endothermal peak. These temperatures were then corrected for the finite heating rate. Slow heating and cooling rates were also used in rheology (0.3 K/min), where we monitored the storage and loss moduli at isochronal conditions (1 rad/s) following isothermal/isochronal crystallization studies at different final temperatures. A representative result from the isochronal runs is shown in Figure 4 for the SEL-4.7/20/1.8 sample. The sample was first quenched from a starting temperature ($T_i$ = 353 K) to different final temperatures, where it was set to crystallize. During the isothermal crystallization the modulus increased from about 1 Pa to 2 × $10^7$ Pa, indicating the transformation from the melt to the crystalline superstructure. Subsequently, heating runs (at 1 rad/s) were performed with the aim to melt the crystal structure. The melting temperatures were obtained from the decrease of the storage modulus upon melting. There was a single (apparent) melting temperature for all samples investigated, as there was a single endothermal peak in the DSC experiment, even when both blocks crystallized. It is the closeness of the equilibrium melting temperatures of PEO and PCL which gives rise to the single, albeit reduced, melting temperature in the stars.

Clearly, there is a dependence of the (apparent) melting temperature on the crystallization temperature, which is a common feature of crystals away from equilibrium. To obtain the equilibrium melting temperature ($T_m^0$), we have used the known Hoffman−Weeks method;[1,2,23] the apparent melting temperature $T_m'$ from both experiments is plotted as a function of the corresponding crystallization temperature $T_c$, and $T_m^0$ is obtained by extrapolation (Figure 5). This procedure results in equilibrium melting temperatures within the range 330−333 K in the stars. These values are considerably smaller than the values for the homopolymers of PEO and PCL (MW = 40 000),[24] which are shown in Figure 6. The solid line in the figure indicates the value for the PS−PEO diblock. Evidently, the melting point depression is mainly created by the PS block. The star structure of the copolymers further reduces the melting point, but to smaller extent. In summary, we found that the condition for the PEO or

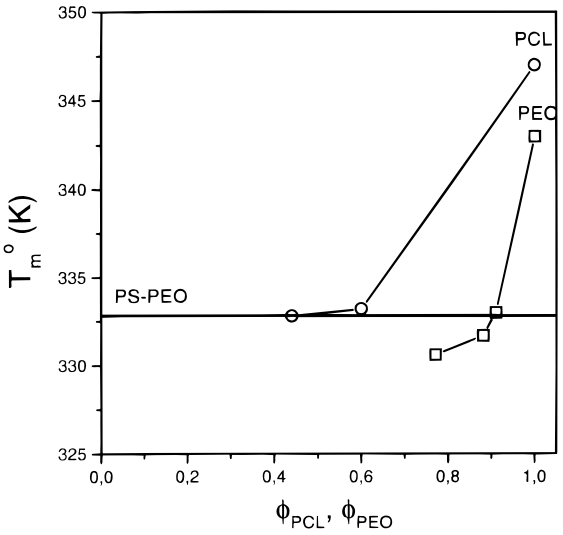


**Figure 6.** Equilibrium melting temperatures obtained from Figure 5 plotted as a function of the PEO and PCL volume fractions in the stars. The solid line gives the equilibrium melting temperature of the diblock PS−PEO.

PCL crystallization in the stars is the value of the block length ratio $N^{PEO}/N^{PCL}$. The crystallinity and crystal thickness are reduced in the stars as compared to the pure components, and when both blocks crystallize, the crystallinity of PCL is less than half the PEO crystallinity. This structural information will be used as input for the crystallization kinetics, below.

**Crystallization Kinetics.** There are different methods which can be employed to study the crystallization kinetics in semicrystalline materials; calorimetry, optical microscopy, dilatometry, simultaneous SAXS/WAXS, and more recently rheology have been employed for this purpose. Here we report on the crystallization kinetics as studied by the first two methods. The calorimetric experiments were performed by heating the samples to the initial temperature $T_i = 348$ K followed by quenches to different final temperatures below the equilibrium melting point. The results from such kinetic experiments are shown in Figures 7 and 8 for the PS−PEO-4.7/20 diblock and SEL-4.7/20/87 star, respectively. We have monitored the crystallization peak (exotherm) as it develops with time. The exothermal peak was integrated in slices so as to obtain the crystallinity $X(t)$ according to

$$1 - X(t) = \frac{\Delta H_\infty - \Delta H_t}{\Delta H_\infty - \Delta H_0} \tag{3}$$

where $\Delta H_\infty$ and $\Delta H_t$ are the latent heats after $t$ and on complete crystallization ($t = \infty$). The analysis of $X(t)$ was based on the Avrami theory,[25] which treats the primary crystallization and growth of spherulites. During primary crystallization, one can assume, to a first approximation, that the degree of crystallinity within the spherulites is constant. The theory takes into account the impingement of the morphological units (spherulites) which have statistically distributed centers. The fraction of molecules transformed into spherulites is then given by

$$1 - X(t) = e^{-zt^n} \tag{4}$$

where $z$ is the rate constant and $n$ is a combined function of the number of dimensions in which growth

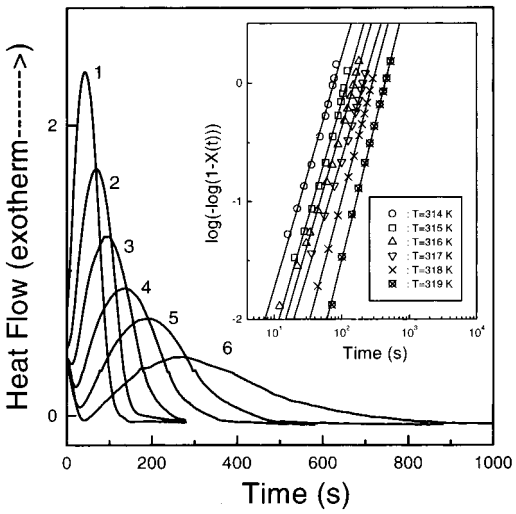


**Figure 7.** Isothermal crystallization of PEO in the diblock PS−PEO-4.7/20 obtained with DSC. The sample was first heated to 348 K and quenched to different final temperatures in the range 314−319 K. The inset gives the Avrami plot for the volume fraction of crystalline material $X(t)$ at different crystallization temperatures (K): (1, ○) 314, (2, □) 315, (3, △) 316, (4, ▽) 317, (5, ×) 318, (6, ⊗) 319. The solid lines are fits to the Avrami equation with $n = 2 \pm 0.1$.

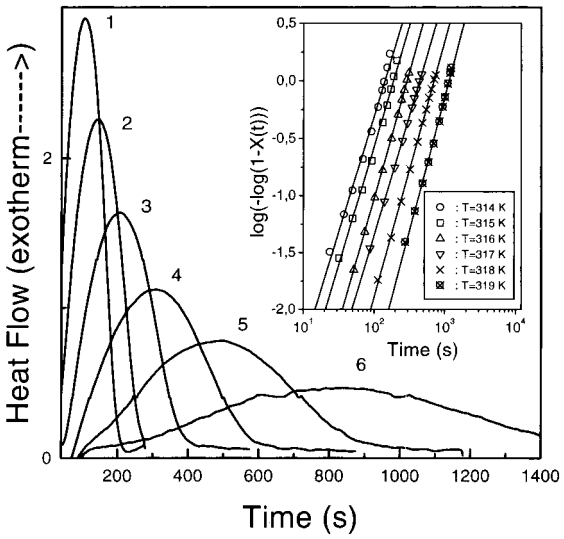


**Figure 8.** Isothermal crystallization in the star block copolymer SEL-4.7/20/87 obtained with DSC. The sample was first heated to 348 K and quenched to different final temperatures in the range 314−319 K. The inset gives the Avrami plot for the volume fraction of crystalline material $X(t)$ at the different crystallization temperatures: (1, ○) 314, (2, □) 315, (3, △) 316, (4, ▽) 317, (5, ×) 318, (6, ⊗) 319. The solid lines are fits to the Avrami equation with $n = 2.2 \pm 0.1$.

takes place and of the order of the time dependence of the nucleation process: homogeneous ($n \propto t^{1.0}$) vs heterogeneous ($n \propto t^0$) process. The rate constant $z$ provides a quantitative check of the course of crystallization, and normally the half-time of the process is used:

$$t_{1/2} = \left(\frac{\ln 2}{z}\right)^{1/n} \tag{5}$$

which is a combined function of $z$ and $n$. Therefore, a comparison of the rates from different processes is meaningful only if $n$ is constant. Alternatively, the exponent $n$ provides only qualitative information on the

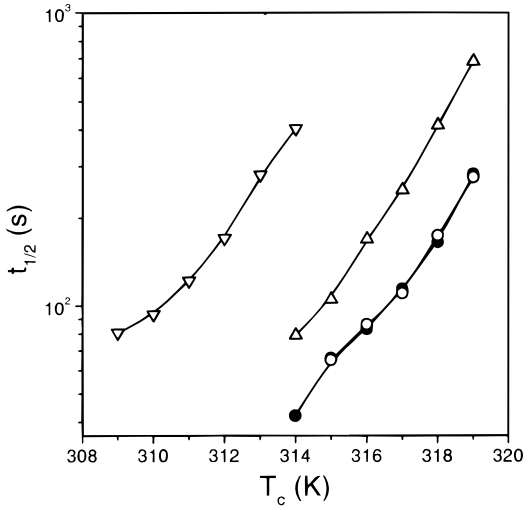


**Figure 9.** Characteristic crystallization times plotted as a function of the crystallization temperature for the diblock PS−PEO and three stars: (●) PS−PEO 4.7/20, (○) SEL-4.7/20/1.8, (△) SEL-4.7/20/87, (▽) SEL-4.7/20/45.

nature of the nucleation and growth process; $n = 3$ implies either a spherulitic growth from heterogeneous nuclei or a disklike growth from homogeneous nuclei. Similarly, $n = 2$ implies either disklike (lamellar) growth from heterogeneous nuclei or rodlike growth from homogeneous nuclei.

The results of the Avrami analysis are shown in the insets of Figures 7 and 8 for the PS−PEO-4.7/20 and SEL-4.7/20/87 samples, which indicate straight and parallel lines, implying a uniform crystallization mechanism. The lines are fits to the Avrami equation, and the resulting values of $n$ were $2 \pm 0.1$, $1.9 \pm 0.1$, $2.2 \pm 0.1$, and $1.9 \pm 0.2$ for the samples PS−PEO-4.7/20, SEL-4.7/20/1.8, SEL-4.7/20/87, and SEL-4.7/20/45, respectively. A value of $n \approx 2$ here implies a planar disklike growth from heterogeneous nuclei for all the samples investigated. Notwithstanding the similarity in the $n$ values, the characteristic times, $t_{1/2}$, differ considerably. The comparison is made in Figure 9 at the different crystallization temperatures. The formation of a star with the introduction of a short PCL block to the PS−PEO diblock (SEL-4.7/20/1.8) has only minor effects on the crystallization kinetics of the PEO block. Introducing a long PCL block (SEL-4.7/20/87) slows down the kinetics of the (PCL) crystallization considerably, but the slowest process occurs in the case of SEL-4.7/20/45 where both blocks can crystallize. In the latter case, chain diffusion necessary for the formation of superstructures (see below) is slowed down by an order of magnitude as compared to the PS−PEO diblock. It is possible that the crystallization of both blocks requires transport of chains over long distances, as compared to the molecular size, and possibly leads to heterogeneous structures (see below). Earlier theoretical[26] and experimental[27] studies have indicated that the mean diffusion length increases as $\Delta T$ decreases ($\Delta T$ is the supercooling) and can be much longer than the molecular size.

A main disadvantage of this technique (DSC), however, is that, without prior information on the structure, it is impossible to infer which one (or if both) of the blocks is crystallizing. This is especially true in the present case with the similar equilibrium melting points of PEO and PCL. Optical microscopy (see below) and simultaneous SAXS/WAXS measurements are required to address this question. We have performed both experiments, and we report here on the results from the optical microscopy measurements (the detailed description of the synchrotron SAXS/WAXS measurements will be reported in a subsequent publication[21]).

The optical measurements were made by continuous monitoring of the crystallizing superstructures following quenches to different crystallization temperatures. We first investigated the crystallization of the pure PEO and PCL and found that upon crystallization different superstructures are formed: spherulites and axialites, respectively. In the block copolymer stars we found that spherulites (axialites) were formed when PEO (PCL) was the majority component and the length ratio of PEO to PCL was 3 or higher. For the stars with comparable block lengths, both spherulites *and* axialites were observed. This finding is in good agreement with the WAXS results, which have shown the possibility that both blocks can crystallize. We interpret the axialitic (spherulitic) superstructure in the stars as composed primarily from PCL (PEO) crystals. This picture implies a very heterogeneous distribution of star molecules; in one population only the PCL blocks can crystallize and the PEO blocks remain amorphous notwithstanding the large supercooling; in the other population, only the PEO blocks can crystallize and the PCL blocks remain amorphous. This crystal selection mechanism results in a kind of macrophase separation between unlike crystals (i.e., crystallization-driven macrophase separation) and probably results in the slow kinetics shown in Figure 9. To check this point further, we have investigated the optical micrographs (see Figure 10 below) with respect to the nucleation sites for the PCL axialites and the PEO spherulites. We found that the nucleation sites of spherulites were much fewer and completely independent from the position of the axialites, indicating a heterogeneous distribution of PEO- and PCL-like crystal sites.

The different shapes of the superstructures provide an efficient way to study the crystallization kinetics by optical microscopy. We have followed the increase of the spherulitic radius and of the long and short axes of axialites with time. In any case, the dependence of the radial and axial growth on time was linear and the growth rates were obtained from the slopes (in the case of axialites, we have used an average growth rate from the long and short axes). Some representative optical micrographs for the SEL-4.7/20/10 sample are shown in Figure 10 (top). The sample, which was initially at 343 K, was quenched to 313 K, and the growth of superstructures was monitored after 11, 14, and 15 min. At 11 min, only PCL axialites exist which grow with a very slow rate as indicated by the small increase in size at the later intervals. At about 14 min, the PEO blocks start to crystallize and the crystallization front moves rapidly and completely fills the space. This shows that the PEO crystal growth is much faster as compared to PCL. Furthermore, we have investigated the effect of annealing at temperatures intermediate between the melting points of the PEO and PCL. We found that melting the sample in the vicinity of the PEO melting temperature, and subsequently quenching to 313 K, results in the formation of PEO spherulites only (Figure 10, bottom). In the case of axialites, we have investigated the dependence of asphericity on the crystallization temperature and found that the higher the supercooling, the smaller the departure from spherulitic structure; for example, in SEL-4.7/20/87 and for a supercooling of 25 K the ratio of the growth velocities is 1.5 as compared to 3 for a supercooling of 15 K.

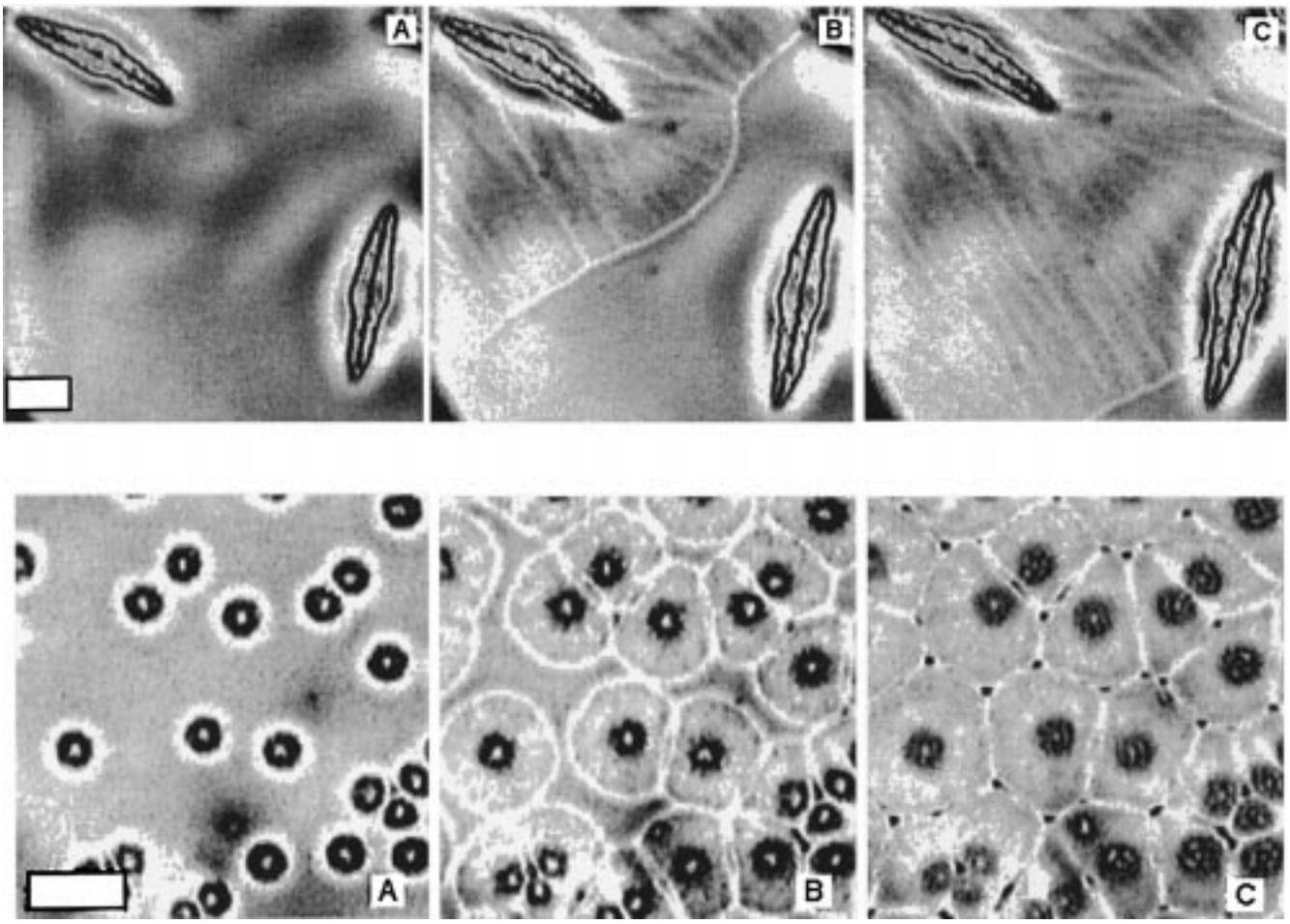


**Figure 10.** Top: Optical micrographs showing the crystallization of PCL and PEO in the star SEL-4.7/20/10. The sample was initially at 343 K and then cooled to 313 K, where it was kept for (A) 11, (B) 14, and (C) 15 min. The axialitic superstructure reflects the crystallization of the PCL block. In parts B and C there is a rapidly moving (spherulitic) crystallization front from the PEO blocks. The bar in the lower left corner indicates 25 $\mu$m. Bottom: Optical micrographs of the same sample obtained through a different history. The sample was heated to 328 K and then cooled to 317 K within 80 s. Picture (A) was taken immediately after *T* arrived at 317 K, picture (B) 12 s later, and picture (C) 1 min later. The circular spherulites indicate the crystallization of the PEO blocks. The bar in the lower left corner indicates 25 $\mu$m.

However, the axialitic shape in the stars was preserved at all temperatures investigated, in contrast to the PCL homopolymer.

The resulting growth rates for PEO, PCL, and the stars are plotted in Figure 11 as a function of the crystallization temperature. Clearly, there is a large difference in growth rates between the pure components, and this provides the means to separate the different rates in the block copolymer stars. The effect of the amorphous PS block in the PS−PEO diblock is to slow down the growth rate as compared to the bulk PEO. Introducing a short PCL block to form the SEL-4.7/20/1.8 star has nearly no effect on the spherulitic growth rate. In the case of SEL-4.7/20/87, the growth of axialites is somewhat faster than that of the pure PCL at the same crystallization temperatures and similar to the growth rates of axialites in SEL-4.7/20/45. For SEL-4.7/20/10, where PEO and PCL crystallization results in the formation of spherulites and axialites, respectively, the two growth rates were modified; axialites grew with a rate similar to that of the pure PCL, whereas spherulites grew with a rate intermediate between PEO and PCL. As we discussed earlier, the two growing superstructures reflect different regions where only PEO crystals are formed and PCL remains amorphous and others where only PCL crystals could be formed by suppressing the crystallization of the PEO.

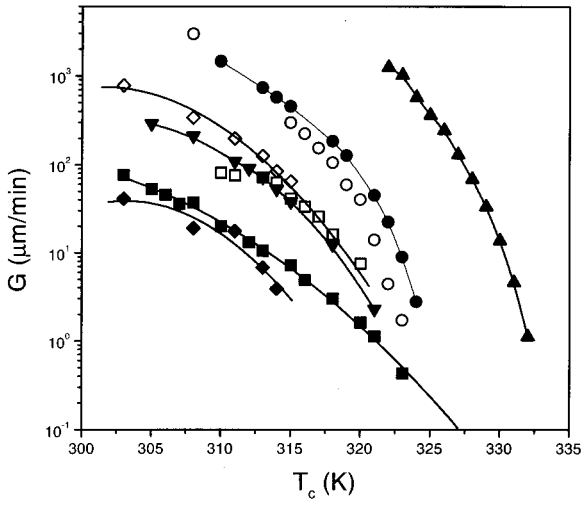


**Figure 11.** Growth rates of spherultites and axialites as a function of crystallization temperature for the different samples: (▲) PEO (spherulites), (■) PCL (axialites), (●) PS−PEO (spherulites), (○) SEL-4.7/20/1.8 (spherulites), (◇) SEL-4.7/20/10 (spherulites), (◆) SEL-4.7/20/10 (axialites), (□) SEL-4.7/20/45 (axialites), (▼) SEL-4.7/20/87 (spherulites).

We have analyzed the growth rates of Figure 11 using the crystallization theory of Lauritzen and Hoffman[28] (crystal growth by secondary nucleation), which is the most accepted approach to analyze the linear growth rates and which has a molecular basis in that it accounts for the diffusion and crystallization of chains. The crystal growth rate is generally given by

$$G \approx G_0 \exp\left(-\frac{E + \Delta F}{kT}\right) \tag{6}$$

where $G_0$ is the growth rate constant, $E$ is the activation energy for transport of crystallizing units across the crystal−liquid interface, and $\Delta F$ is the free energy required to form a nucleus of critical size on the face of a crystal. The first and second terms in the above equation can be modified to take into account the known activation parameters as

$$G(i) = \frac{z}{N^v} \exp\left(-\frac{E}{R(T_c - T_\infty)}\right) \exp\left(\frac{-K_g(i)}{T_c \Delta T f}\right) \tag{7}$$

where $z$ is a parameter containing mobility terms, $N$ is the degree of polymerization, and the value of the exponent $v$ depends on the growth regime (see below), $T_c$ is the crystallization temperature, $T_\infty$ is the ideal glass transition temperature ($=T_g - 30$ (K)), $\Delta T$ is the supercooling ($=T_m^0 - T_c$), $f$ is a temperature correction factor for the heat of fusion ($=2T_c/(T_m^0 + T_c)$), and $K_g(i)$ is the nucleation rate constant given by

$$K_g = \frac{ib_0\sigma\sigma_e T_m^{\,0}}{k\Delta H_f} \tag{8}$$

where $b_0$ is the width of the chain, $\sigma$ is the lateral surface free energy, $\sigma_e$ is the fold surface free energy, and $\Delta H_f$ is the heat of fusion. The symbol $i$ represents a number associated to the particular regime and is equal to 4 for regimes I and III and equal to 2 for regime II.[22,29] The three regimes differ according to the competition between the rate of deposition of secondary nuclei ($d$) and the rate of lateral surface spreading ($g$); in regime I, $d \ll g$ and appears at very low supercoolings, in regime II, $d \approx g$ and occurs for intermediate supercooling, and in regime III, $d > g$ and corresponds to very high supercoolings.

The main advantage of this theory is that it allows for the calculation of the surface free energy product $\sigma\sigma_e$ from which valuable information on the purity of crystal structures can be obtained. Taking the natural logarithm of eq 7 and plotting $\ln G(i) - \ln \Delta T + E/R(T_c - T_\infty)$ vs $(T_c\Delta T f)^{-1}$, we can extract the nucleation rate constant from the slope. The result of the analysis is shown in Figure 12 for PEO, PCL, the diblock PS−PEO, and the stars. For all samples there is a single slope, indicating a single regime. From the data sets shown in the figure there is a clear distinction between the slope of the bulk PCL and that of the rest of the samples. For PCL, despite the nonspherulitic morphology, earlier optical microscopy measurements have shown that the data correspond to regime II.[24] In evaluating the slopes from Figure 12, we have also assumed regime II and used $E^{PCL} = 1500$ cal/mol, $T_g^{PCL} = 210$ K, $\Delta H_f = 1.5 \times 10^9$ erg/cm$^2$, and $b_0 = 4.12$ Å (for the latter we assumed a situation analogous to polyethylene, with the (110) growth front). Using these parameters, we obtained 625 erg$^2$/cm$^4$ for the product $\sigma\sigma_e$, a value which is in good agreement with literature values.[24] For the PEO spherulites in the bulk PEO, the diblock PS−PEO, and the stars, which showed spherulitic superstructure, the following parameters were used: $E^{PEO} = 1500$ cal/mol, $T_g^{PEO} = 206$ K, $\Delta H_f = 2.31 \times 10^9$ erg/cm$^2$, and $b_0 = 4.54$ Å.[24] The product $\sigma\sigma_e$ for PEO was 274 erg$^2$/cm$^4$, which is also in good agreement with the reported values for PEO corresponding to regime II.[8,22] Regime II appears to apply for all samples investigated, and the values for

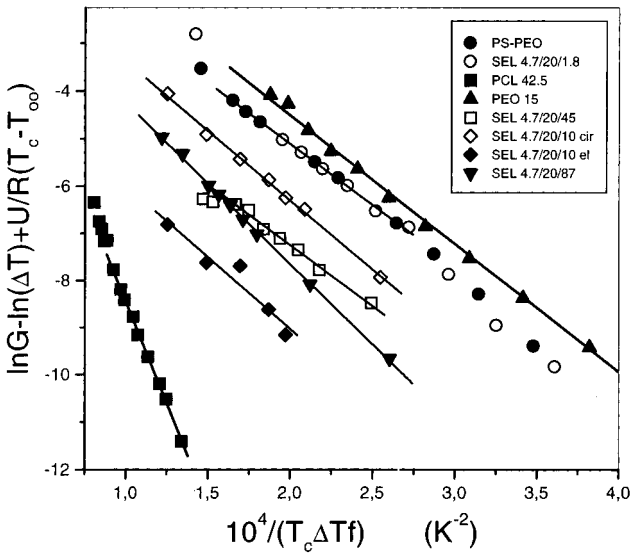


**Figure 12.** Growth rates for spherulites and axialites as a function of reduced temperature. The symbols are the same as those in Figure 11.

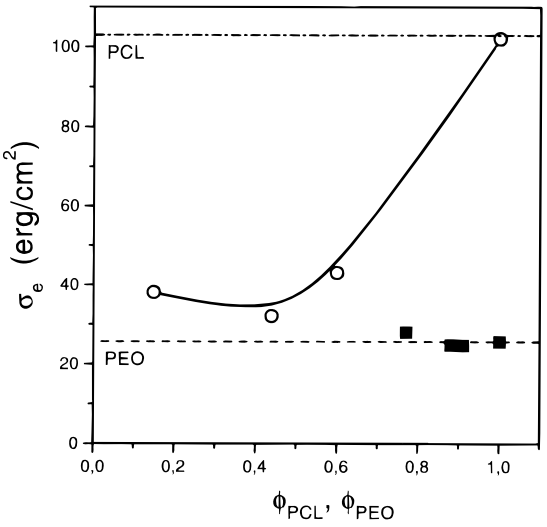


**Figure 13.** Fold surface free energy plotted as a function of the volume fraction of PEO and PCL. The dashed and dash−dotted lines give the value for the bulk PEO and PCL, respectively.

**Table 3. Nucleation Constant and Surface Free Energy Product Obtained from the Slopes of Figure 12**

| sample | $K_g$ (K$^{-2}$) | $\sigma\sigma_e$ (erg$^2$/cm$^4$) |
|---|---|---|
| PEO-15 | −27 135 | 274 |
| PCL-42.5 | −85 890 | 625 |
| PS−PEO-4.7/20 | −25 660 | 264 |
| SEL-4.7/20/1.8 | −25 660 | 265 |
| SEL4.7/20/45 | −25 870 | 196 |
| SEL-4.7/20/87 | −34 990 | 265 |
| SEL-4.7/20/10 (spherulites) | −29 240 | 298 |
| SEL-4.7/20/10 (axialites) | −30 530 | 233 |

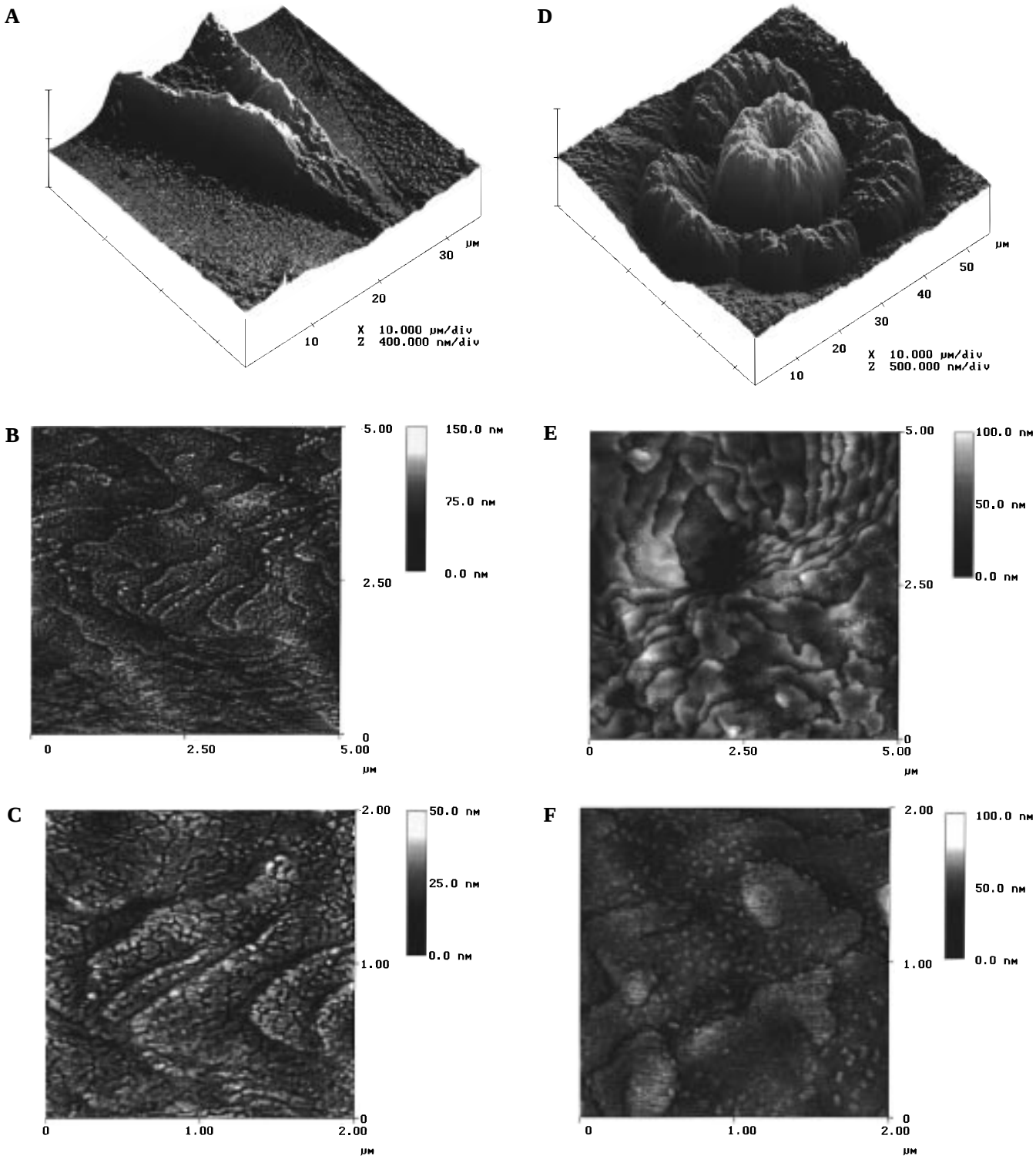


**Figure 14.** Atomic force microscopy topography images obtained from a 150-nm-thick film of SEL-4.7/20/10. Images A−C: the sample was first heated to 343 K and then cooled to 308 K, kept there for 3 min, and reheated to 321 K, where it was kept for 40 min. The sample was then quenched to room temperature (RT). Images D−F: the same sample was only heated to 329 K, then cooled to 319 K, where it was kept for 10 min, and finally quenched to RT. The height images B, C, E, and F have been flattened and slightly contrast-enhanced to improve the visibility of the patterns.

the surface free energy product are summarized in Table 3.

The main finding from the results shown in Table 3 is that the surface free energy product attains values similar to those of pure PEO even when the growing superstructure is axialitic (SEL-4.7/20/10). To investigate this seemingly paradoxial situation, we need to separately discuss the values of the lateral and fold surface free energies. For this purpose we employ the Thomas−Stavely relation[30] for the lateral surface free energy:

$$\sigma = 0.1\Delta H_f b_0 \tag{9}$$

assuming the same $b_0$ values corresponding to regime II. The resulting values of $\sigma_e$ are plotted in Figure 13

as a function of the volume fraction of the crystallizable blocks. In the same figure we plot with dashed and dash−dotted lines the values of bulk PEO and PCL, respectively. PEO and PCL have similar mobility parameters (i.e., glass temperatures and activation energies), but their crystals have very different fold surface free energies and this difference is used here as a tool for obtaining information on mixing at the fold surface. Clearly, the PEO spherulites are formed by nearly pure PEO crystals, and no mixing occurs between the fold surface and the amorphous PS and PCL blocks. On the contrary, the PCL axialites are formed by PCL crystals which are mixed with PS and possibly with the amorphous PEO blocks at the fold surface.

The picture emerging from the above kinetic studies is the following: at high $T$, the blocks form a homogeneous phase. Upon cooling crystallization of one (or both) blocks sets in, which drives the microphase separation in the system. However, when both blocks undergo crystallization, this is not happening within the same molecule. The PEO crystals thus formed are nearly pure; however, the PCL blocks remain mixed with the PS blocks. The mixing within the PCL phase inhibits a uniform crystallization and reduces the crystallinity of the PCL phase. These results are supported by the AFM studies below.

AFM topography images were obtained from an approximately 150-nm-thick film of SEL-4.7/20/10. In Figure 14, images A−C, the sample was first heated to 343 K and then cooled to 308 K, kept there for 3 min (to facilitate the primary nucleation of crystals), and reheated to 321 K, where it was kept for 40 min (to observe crystal growth). The sample was then quenched to room temperature (RT). In D−F the same sample was heated only to 329 K, then cooled to 319 K where it was kept for 10 min, and finally quenched to RT. In A−C only PCL could crystallize, indicated by the elongated shape of the pattern (see A, where this pattern is embedded in a rather smooth film crystallized rapidly at RT). These axialites grow also in the direction normal to the surface by piling up perforated lamellae (see B and C: these height images have been flattened and slightly contrast-enhanced to improve the visibility of the patterns). We assume that the PEO and PS blocks cannot be forced to stay on top of the PCL lamellae because (lateral) forces of entropic origin due to the massive stretching, in particular of the longer PEO blocks (these may be thought to form a "brushlike" structure on top of the PCL lamellae), tend to rupture the PCL crystals. Consequently, the PCL lamellae contain a significant number of "cracks" or perforations, probably partially occupied by amorphous PEO and/or PS blocks. This simple model has to be contrasted to the result when PEO crystallizes (see D−F). Here the crystalline region (grown at 319 K) has a circular shape. There is also growth in the vertical direction. Lamellar sheets are piled up with increasing inclination in the growth direction. At a diameter of about 15 $\mu$m, the lamellae are almost vertically oriented. At a larger diameter (i.e., at later stages of crystallization), the lamellae become less tilted, and at a diameter of about 30 $\mu$m, they are oriented almost parallel to the substrate. This repeated "stacking of sheets" results in the flowerlike pattern seen in D. The sheets are continuous (absence of cracks), and at the surface, dropletlike features can be seen (see E and F: again these height images have been flattened and slightly contrast-enhanced to improve the visibility of the patterns). We suppose that the PEO lamellae are coated with a brushlike structure formed by the PS and PCL blocks. The "droplets" at the surface may well be due to a coalescence of PCL and/or PS blocks to form micellar aggregates on the order of 30−50 nm in diameter. Such an interpretation of the AFM images is in agreement with the results from WAXS (Figure 2) and optical microscopy (Figure 13).

However, despite the general agreement among the results from X-rays, optical microscopy, and atomic force microscopy, there are still many unresolved issues. For example, the suppression of crystallization in the stars and the role of the film thickness[31,32] on the nucleation density, crystal growth, and crystallinity in relation to chain topology (star architecture) require further investigation. We are currently working in this direction.

## Conclusions

We have studied the structure and crystallization in triarm star block copolymers composed of two crystallizable blocks. Crystallization starts from the homogeneous melt phase and drives the microphase separation. This study is facilitated by the different unit cells and specific area requirements of PEO and PCL crystals. The main findings of the present investigation are as follows:

1. Both blocks can crystallize in the stars provided that their length ratio is below 3. However, this does not necessarily imply that the two blocks crystallize within the same molecule. For the more asymmetric stars, the longer block completely suppresses the crystallization of the shorter one.

2. The crystallinity, long period, and crystalline lamellar thickness are reduced in the stars as compared to the pure PEO and PCL. Furthermore, when both PEO and PCL crystallize, the crystallinity of the PCL phase is reduced to about half the value of the PEO phase.

3. The reduction in the equilibrium melting temperature in the stars is caused primarily by the amorphous PS block. The star structure reduces the $T_m^0$ further, but to a smaller extent.

4. The Avrami analysis of the isothermal crystallization calorimetric experiments indicated a disklike growth from heterogeneous nuclei, independent of the nature of the crystallizing block. However, the crystallization times were sensitive to the nature of the crystallizable block, and when both blocks crystallized, the kinetics were slowed down with respect to the pure components.

5. Different superstructures were formed (spherulites/axialites) depending on the type of crystallizable block (PEO/PCL). The nucleation sites of the two superstructures were completely independent, suggesting a heterogeneous distribution of star molecules with PEO or PCL crystals. This heterogeneous distribution implies the existence of a kind of macrophase separation between unlike crystals.

6. From the growth rates of the superstructures, the fold surface free energies were obtained and indicated a pure PEO crystal but a perforated PCL crystal. This conclusion was supported by the results of the AFM in thin films.

**Acknowledgment.** This work was supported by a French−Greek collaborative grant (CNRS-NHRF (1998)) to G.R. and G.F.

## References and Notes


(1) Wunderlich, B. *Macromolecular Physics 2. Crystal Nucleation, Growth, Annealing*; Academic Press: New York, 1978.
(2) Strobl, G. *The Physics of Polymers*; Spinger-Verlag: Berlin, 1996; Chapter 4.
(3) Leibler, L. *Macromolecules* **1980**, *13*, 1602.
(4) Floudas, G.; Pispas, S.; Hadjichristidis, N.; Pakula, T.; Erukhimovich, I. *Macromolecules* **1996**, *29*, 4142.
(5) Lotz, B.; Kovacs, A. J.; Bassett, G. A.; Keller, A. *Kolloid Z. Z. Polym.* **1966**, *209*, 115.
(6) Lovinger, A. J.; Han, B. J.; Padden, F. J.; Mirau, P. A. *J. Polym. Sci., Polym. Phys. Ed.* **1993**, *31*, 115.
(7) Rangarajan, P.; Register, R. A.; Fetters, L. J. *Macromolecules* **1993**, *26*, 4640.
(8) Richardson, P. H.; Richards, R. W.; Blundell, D. J.; MacDonald, W. A.; Mills, P. *Polymer* **1995**, *36*, 3059.
(9) Rangarajan, P.; Register, R. A.; Fetters, L. J.; Bras, W.; Naylor, S.; Ryan, A. J. *Macromolecules* **1995**, *28*, 1422.
(10) Hamley, I. W.; Fairclough, J. P. A.; Ryan, A. J.; Bates, F. S.; Towns-Adrews, E. *Polymer* **1996**, *37*, 4425.
(11) Floudas, G.; Tsitsilianis, C. *Macromolecules* **1997**, *30*, 4381.
(12) Perret, R.; Skoulios, A. *Makromol. Chem.* **1972**, *162*, 147; **1972**, *162*, 163.
(13) Gan, Z.; Jiang, B.; Zhang, J. *J. Appl. Polym. Sci.* **1996**, *59*, 961.
(14) Lambert, O.; Dumas, P.; Hurtez, G.; Riess, G. *Macromol. Rapid Commun.* **1997**, *18*, 343. Lambert, O.; Reutenauer, S.; Hurtez, G.; Riess, G.; Dumas, P. *Polym. Bull.* **1998**, *40*, 143.
(15) Herman, J.-J.; Jerome, R.; Teyssie, P.; Gervais, M.; Gallot, B. *Makromol. Chem.* **1981**, *182*, 997.
(16) Li, Y.; Jungnickel, B.-J. *Polymer* **1993**, *34*, 9.
(17) Floudas, G.; Hadjichristidis, N.; Iatrou, H.; Pakula, T.; Fischer, E. W. *Macromolecules* **1994**, *27*, 7735.
(18) Olvera de la Cruz, M.; Sanchez, I. C. *Macromolecules* **1986**, *19*, 2501.
(19) Tadokoro, H.; Chatani, Y.; Yoshihara, T.; Tahara, S.; Murahashi, S. *Makromol. Chem.* **1964**, *73*, 109.
(20) Chatani, Y.; Okita, Y.; Tadokoro, T.; Yamashita, Y. *Polym. J.* **1970**, *1*, 555.
(21) Floudas, G.; Reiter, G.; Lambert, O.; Dumas, P.; Chu, B., in preparation.
(22) Mezghani, K.; Phillips, P. J. *Physical Properties of Polymers Handbook*; Mark, J. E., Ed.; AIP Press: Woodbury, NY, 1996.
(23) Recent experiments on copolymers based on polypropylene indicated that the Hoffman−Weeks method may not be exact: Strobl, G. Personal communication. In fact, the validity of this approach has been questioned even for homopolymers: Schmidtke, J.; Strobl, G.; Thurn-Albrecht, T. *Macromolecules* **1997**, *30*, 5804. However, no alternative procedure to extract the equilibrium melting point has been provided.
(24) Phillips, P. J.; Rensch, G. J.; Taylor, K. D. *J. Polym. Sci., Polym. Phys. Ed.* **1987**, *25*, 1725.
(25) Avrami, M. J. *J. Chem. Phys.* **1939**, *7*, 1103; **1940**, *8*, 212; **1941**, *9*, 177.
(26) Goldenfeld, N. *J. Cryst. Growth* **1987**, *84*, 601. Keith, H. D.; Padden, F. J. *J. Appl. Phys.* **1963**, *34*, 2409.
(27) Reiter, G.; Sommer, J.-U. *Phys. Rev. Lett.* **1998**, *80*, 3771.
(28) Lauritzen, J. I.; Hoffman, J. D. *J. Res. Natl. Bur. Stand.* **1960**, *64A*, 73.
(29) Lovinger, A.; Davis, D. D.; Padden, F. J. *Polymer* **1985**, *26*, 1595.
(30) Thomas, D. G.; Stavely, L. A. K. *J. Chem. Soc.* **1962**, 4569.
(31) Frank, C. W.; Rao, V.; Despotopoulou, M. M.; Rease, R. F. W.; Hinsberg, W. D.; Miller, R. D.; Rabolt, J. F. *Science* **1996**, *273*, 912.
(32) Despotopoulou, M. M.; Frank, C. W.; Miller, R. D.; Rabolt, J. F. *Macromolecules* **1996**, *29*, 5797.


MA9806716